Mass distributions in the reaction of 240 MeV ^{12}C with ^{197}Au

H. Kudo,* K. J. Moody,† and G. T. Seaborg
Nuclear Science Division, Lawrence Berkeley Laboratory, University of California, Berkeley, California 94720
(Received 16 January 1984)

The mass distributions of fission products and targetlike products in the reaction of 20 MeV/nucleon ^{12}C with ^{197}Au were determined radiochemically. The charge dispersions of the fission products were found to have Gaussian shapes with a width parameter ($2\sigma^2$) of 1.6 units and a most probable charge of $0.417A+1.4$. As for near- and above-target products, the broad charge dispersions of $A=196$ to 199 suggest contributions from two mechanisms, one corresponding to a quasielastic process and the other corresponding to deeply inelastic and/or complete fusion processes. The cross sections of above-target products were larger than the values expected from simple evaporation calculations.

I. INTRODUCTION

It is interesting to study how the reaction mechanisms in heavy-ion-induced reactions vary with incident projectile energy, especially for energies near the nuclear Fermi energy. In recent years, heavy ion beams of intermediate energy have become available for these experiments.

A radiochemical experiment usually aims at defining what occurs during a nuclear reaction by observing the change induced in a heavy target nucleus. These techniques were used in much of the early work with low energy reactions (a few MeV/nucleon), where typical reaction processes are elastic scattering, quasielastic scattering, deeply inelastic scattering, complete fusion, and incomplete fusion. Similarly, in high energy heavy-ion reactions (hundreds of MeV/nucleon or more), radiochemical measurements of forward-backward ratios, charge dispersions, and mass distributions of residual nuclei[1–6] have helped develop the picture of a fast abrasive step followed by thermalization and deexcitation of the primary reaction products.

There is little published radiochemical work in the intermediate energy region. Most experiments performed at these energies have involved the measurement of the energy spectra of light emitted fragments which are interpreted with a moving source model,[7–9] a preequilibrium exciton model,[10,11] the nuclear fireball model,[11] etc. Symons *et al.*[11] have used both a low energy model and a high energy model to try to explain the energy spectra of protons in the system of 20 MeV/nucleon $^{16}O+^{197}Au$. Egelhaaf *et al.*[12] have concluded that, in the system of 20 MeV/nucleon $^{20}Ne+^{197}Au$, incomplete fusion and sequential decay occur in addition to complete fusion and ordinary transfer reactions, and that other mechanisms do not contribute significantly.

In this work, we have examined the mass distribution of 20 MeV/nucleon $^{12}C+^{197}Au$ using radiochemical methods. We have chemically isolated both fission products and near-target products. Results have been compared with an evaporation calculation assuming the formation of a compound nucleus, and including preequilibrium processes via the exciton model.

II. EXPERIMENTAL

A. Irradiations

The experimental irradiations were performed at the Lawrence Berkeley Laboratory's 88-Inch Cyclotron. The gold targets for most of the determinations consisted of uniform, self-supporting gold foils of 5.16 mg/cm^2 thickness, mounted between two pieces of 6.24 mg/cm^2 aluminum foil (99.99% purity) to completely collect both forward and backward recoil products. An additional 6.24 mg/cm^2 aluminum foil in the forward direction was used to isolate the target foils from nuclides produced in the beam stop. For experiments where products which decayed by alpha particle emission were measured (discussed in the following), the thickness of the gold foil varied from 1 to 2 mg/cm^2, and the aluminum catcher foils were 1.8 mg/cm^2, sufficient to stop complete fusion recoils.[13]

The target foils were bolted to a copper block at the back of an electron-suppressed Faraday cup and were irradiated with 245 MeV $^{12}C^{5+}$ with an average intensity of about 20 electrical nanoamperes. The aluminum catcher foil in the backward direction degraded the energy of the beam to 240 MeV.[13] The diameter of the beam spot was 10 mm, defined with an upstream graphite collimator. The irradiation times for each experiment varied from 5 min to 12 h, depending upon the half-lives of the nuclides which were of interest. The beam current entering the Faraday cup was measured with an electrometer, and the integral was recorded periodically to permit accurate beam flux histories to be constructed.

To estimate the possible effect of charged-particle-induced secondary reactions on the measured reaction cross sections, a set of targets with different thicknesses between 1.0 and 5.16 mg/cm^2 were irradiated. It was found that, within statistics, there was no change in any of the reaction product cross sections as a function of target thickness. We are unable to state that there is no contribution to near-target reaction cross sections from neutrons produced in the thick copper beam stop. However, given the center-of-mass velocity, the thickness of the gold targets, and the cross sections for reactions of neu-

trons with gold,[14] we feel that the only nuclides which may have a significant contribution from neutron-induced reactions are ^{196}Au and ^{198}Au.

B. Chemical separations

Each irradiated gold target with its aluminum cover foils was dissolved in aqua regia with an excess of HCl in a distillation flask containing carriers and/or tracers for the elements of interest. The elements characteristically present as fission products were separated with standard chemical procedures.[15] Brief comments on the separation schemes for the elements near gold are located in the Appendix at the end of this paper. Each run produced three to ten samples. Chemical yields were obtained either by measuring the tracer activities, by weighing the carriers, or by comparison of the most intense activities with those measured from an unseparated target.

Almost all products at a significantly higher Z than that of the target were expected to recoil in the forward (beam) direction. In experiments designed to detect alpha-emitting polonium and astatine isotopes, thin gold foils were used (described previously) that allowed these products to escape to the forward catcher foil. This was checked by surveying an unseparated target and forward foil for gamma-ray activity due to ^{196}Pb and ^{198}Bi. Therefore, for measurements of polonium and astatine alpha activities, the forward aluminum catcher foil was melted on a copper disk and the volatile elements were collected on a copper foil cooled with liquid nitrogen or dry ice. Only alpha activity from polonium isotopes was observed. For more chemical details, see the Appendix.

C. Radioactivity measurements and data treatment

The activity of each product was determined by observing its characteristic gamma rays except for ^{198}Po, ^{199}Po, and ^{200}Po, which were observed via their alpha activity. The gamma-ray spectrometer system was based on four Ge(Li) detectors equipped with pulse-height analyzers. The photoelectric efficiencies of the detectors were determined as a function of gamma-ray energy for a number of well-defined geometries with a set of calibrated radionuclide sources. The energy resolutions (FWHM) of the detectors were 2.00, 2.05, 2.66, and 2.67 keV for the 1332 keV gamma ray of ^{60}Co. The gamma-ray spectrum of each sample in the energy range 50 keV $\leq E \leq$ 2 MeV was measured at a pulse-height analyzer (PHA) gain of 0.5 keV/channel as a function of time for a total period of about two months for each run. For alpha activity measurements, a Si(Au) surface barrier detector was used. The efficiency of this detector was determined with a source containing a known amount of ^{210}Po.

The gamma-ray spectral data were analyzed with the set of computer programs described in Ref. 16. These programs consist of a peak search, fitting, and integrating program (SAMPO), a sorting program for decay curve construction (TAU1), and an interactive decay curve identification program (TAU2). Since the accuracy of the initial activities determined with TAU2 is defined by the accuracy of the isotope table used in the identifications,[17] the intensity of each line was checked against more recent compilations[18,19] to improve the reliability of these data. The end-of-bombardment activities were converted to cross sections taking into account both the appropriate chemical yield and the variation of the beam intensity during the irradiation. Whenever possible, the activities were corrected for precursor decay before the cross section calculation. If several gamma rays of the same nuclide were observed, the cross section was calculated from the weighted average of all the corrected gamma-ray intensities.

III. RESULTS AND DISCUSSION

The cross sections of about 250 nuclides produced in the reaction of 20 MeV/nucleon ^{12}C with ^{197}Au were determined and are tabulated in Table I and plotted in Fig. 1(a). Table I also indicates whether or not a particular cross section is an independent yield, the experimental method by which it was observed, and the half-life and principal gamma-ray energy and intensity used in the cross section calculation.

A. Fission products

Many of the observed fission products were members of the same mass chain so the charge dispersion could be obtained. The shape of the charge dispersion was assumed to be Gaussian,

$$P(Z)=C\exp[-(Z_p-Z)^2/2\sigma^2]\ .$$

The most probable atomic number (Z_p) seems to be well reproduced with the linear equation $Z_p=0.417A+1.4$. The charge dispersions of all fission products (from $71 \leq A \leq 145$) were found to have similar values of the width parameter, $2\sigma^2=1.6$. This is demonstrated in Fig. 2, where all the fission data are scaled and plotted on the same axes.

The width we observe here is rather large compared to those widths arising from processes at lower energy. In the reaction of 112 MeV ^{12}C with ^{197}Au, the width $2\sigma^2$ is 0.9.[20] The widths of the charge dispersions from the low energy fission of uranium range from 0.80 to 0.95.[21,22] The broadening observed here results, in part, from the large variety of primary reaction products which will decay by fission, and partly from the high angular momentum of the fissioning nuclides. The dependence of the width parameter on excitation energy is thought to be small.[22]

The data displayed in Fig. 2 give a measure of the confidence with which the charge dispersions of the fission products can be described with the Z_p and width parameter already detailed. Using these values, the total chain yield for each mass number can be estimated from the available experimental data. The obtained mass distribution is plotted in Fig. 1(b). In this figure, the solid line represents a Gaussian fit to the data points from $A=71$ to 145. The peak of this mass distribution is at $A=95.6$.

TABLE I. Cross sections measured in 20 MeV/nucleon $^{12}C+^{197}Au$.

Nuclide	Cross section (mb)	Type[a]	Method[b]	Half-life	E_γ (keV)	I_γ (%)	Reference
^{71}As	0.299 ± 0.047	*CD*	*C*	2.7 d	174.9	83.1	19
^{72}As	1.06 ± 0.17	*I*	*C,D*	1.083 d	834.0	79.5	19
^{74}As	8.49 ± 1.24	*I*	*C,D*	17.70 d	595.9	59.2	17
^{76}As	14.7 ± 2.1	*I*	*C,D*	1.096 d	559.1	44.6	17
^{77}As	16.3 ± 2.8	*CR*	*C*	1.613 d	239.1	1.6	19
^{78}As	10.1 ± 2.1	*CR*	*C,D*	1.510 h	613.7	54.0	19
^{73}Se	0.288 ± 0.060	*CD*	*C*	7.18 h	360.9	97.	18
^{75}Se	5.08 ± 0.22	*CD*	*C*	118.45 d	264.65	58.	18
$^{81}Se^m$	21.1 ±15.6	*CR*	*C*	57.28 min	102.7	9.7	18
^{82}Br	23.9 ± 6.7	*I*	*D*	1.479 d	698.2	27.9	17
$^{84}Br^m$	7.46 ± 1.13	*CR*	*D*	6. min	1462.8	97.	18
$^{85}Kr^m$	2.99 ± 1.35	*CR*	*D*	4.481 h	151.3	76.1	17
^{88}Kr	12.6 ± 8.3	*CR*	*D*	2.86 h	196.3	26.3	18
$^{82}Rb^m$	2.90 ± 2.30	*I*	*D*	6.5 h	618.9	39.2	19
$^{84}Rb^m$	14.1 ± 4.5	*I*	*D*	20.405 min	247.9	59.	19
$^{84}Rb^g$	3.19 ± 1.86	*I*	*C*	32.77 d	881.6	67.8	19
^{86}Rb	4.66 ± 1.74	*I*	*C*	18.82 d	1077.2	8.79	18
^{83}Sr	1.31 ± 0.34	*CD*	*C*	1.35 d	762.5	29.4	17
$^{85}Sr^m$	0.463 ± 0.148	*I*	*C*	68. min	231.7	84.5	18
$^{85}Sr^g$	13.1 ± 1.1	*I*	*C*	64.85 d	514.	100.	18
^{91}Sr	12.9 ± 3.4	*CR*	*C*	9.5 h	1024.3	33.4	18
^{92}Sr	5.07 ± 0.56	*CR*	*C,D*	2.71 h	1383.9	90.	17
^{93}Sr	0.840 ± 0.200	*CR*	*C*	7.43 min	590.18	66.5	19
$^{85}Y^m$	0.382 ± 0.056	*CD*	*C*	4.9 h	231.7	23.4	19
$^{85}Y^g$	0.109 ± 0.023	*CD*	*C*	2.68 h	504.5	64.	18
$^{86}Y^m$	2.13 ± 1.72	*I*	*C,D*	48. min	208.2	94.	18
$^{86}Y^g$	3.25 ± 0.16	*I*	*C,D*	14.74 h	627.72	32.6	18
$^{87}Y^m$	11.3 ± 2.0	*CD*	*C,D*	13.2 h	381.1	78.	18
$^{87}Y^g$	13.6 ± 2.8	*I*	*D*	80.3 h	484.8	92.	18
^{88}Y	26.3 ± 0.8	*I*	*C*	106. d	898.0	92.	17
$^{90}Y^m$	35.7 ± 6.4	*I*	*C*	3.19 h	202.4	97.	17
$^{91}Y^m$	32.5 ± 2.5	*I*	*D*	49.694 min	555.6	94.9	17
^{92}Y	20.6 ± 6.9	*CR*	*C,D*	3.530 h	934.5	13.7	17
^{93}Y	16.3 ± 2.8	*CR*	*C*	10.2 h	267.	6.8	18
^{94}Y	5.13 ± 0.83	*CR*	*C*	18.7 min	918.8	73.3	19
^{95}Y	3.75 ± 0.68	*CR*	*C*	10.3 min	954.2	13.4	19
^{86}Zr	0.438 ± 0.104	*CD*	*C*	16.5 h	243.0	96.	17
^{87}Zr	0.340 ± 0.315	*CD*	*C*	1.73 h	1228.	3.0	19
^{88}Zr	3.19 ± 0.18	*CD*	*C,D*	85. d	392.8	97.	17
^{89}Zr	10.5 ± 1.6	*CD*	*C*	3.271 d	909.2	100.	17
^{95}Zr	25.3 ± 6.6	*CR*	*C*	64. d	756.7	54.6	18
^{97}Zr	4.73 ± 0.12	*CR*	*C*	16.9 h	743.4	92.8	18
^{90}Nb	3.50 ± 0.76	*CD*	*C*	14.6 h	1129.2	92.6	18
$^{92}Nb^m$	19.7 ±18.4	*I*	*C,D*	10.1 d	934.5	99.1	17
$^{95}Nb^g$	46.8 ± 2.5	*I*	*C,D*	35.1 d	765.8	99.	17
^{96}Nb	35.6 ±10.2	*I*	*D*	23.501 h	1091.3	49.4	17
^{97}Nb	28.0 ± 0.4	*I*	*C,D*	73.62 min	658.1	99.	17
$^{98}Nb^B$	8.23 ± 1.69	*CR*	*D*	51.005 min	787.2	95.	17
$^{93}Mo^m$	3.13 ± 0.09	*CD*	*C*	6.95 h	1477.2	99.1	18
^{99}Mo	38.4 ± 3.1	*CR*	*D*	66.02 h	739.6	12.1	19
^{102}Mo	31.4 ±13.6	*CR*	*D*	11.0 min	475.0	6.3	19
$^{94}Tc^g$	0.623 ± 0.351	*CD*	*C*	293. min	871.01	100.	18
$^{95}Tc^g$	3.32 ± 0.77	*CD*	*C*	20. h	765.8	94.	17
^{96}Tc	6.71 ± 1.60	*I*	*C,D*	4.3 d	849.9	97.8	17
$^{99}Tc^m$	6.96 ± 0.14	*I*	*D*	6.02 h	140.5	89.	18
^{101}Tc	10.2 ± 1.6	*I*	*D*	14.00 min	306.8	88.7	17
$^{102}Tc^m$	15.4 ± 0.8	*I*	*D*	4.35 min	474.8	85.0	18
^{104}Tc	4.95 ± 0.18	*CR*	*D*	18.40 min	357.8	89.0	19
^{97}Ru	1.61 ± 0.14	*CD*	*C,D*	2.89 d	215.7	87.6	17

TABLE I. (*Continued*).

Nuclide	Cross section (mb)	Type[a]	Method[b]	Half-life	E_γ (keV)	I_γ (%)	Reference
^{103}Ru	51.0 ± 1.1	*CR*	*C,D*	39.6 d	497.1	90.	17
^{105}Ru	17.8 ± 0.3	*CR*	*C,D*	4.44 h	469.4	17.5	17
^{100}Rh	2.30 ± 0.13	*I*	*C*	20.8 h	539.6	78.4	18
^{101}Rh^m	5.83 ± 0.24	*CD*	*C,D*	4.34 d	306.8	86.3	19
^{105}Rh	28.3 ± 1.9	*I*	*C*	35.47 h	318.9	19.	18
^{106}Rh^m	14.1 ± 0.4	*I*	*C,D*	130. min	717.2	29.2	18
^{108}RH^B	7.04 ± 3.33	*CR*	*D*	5.9 min	434.2	100.	17
^{100}Pd	0.123 ± 0.009	*CD*	*C*	3.63 d	539.6[f]	78.4	18
^{101}Pd	0.510 ± 0.043	*CD*	*C*	8.47 h	296.29	18.	18
^{109}Pd	25.5 ± 0.5	*CR*	*C*	13.427 h	88.04	3.6	18
^{111}Pd^m	2.87 ± 0.70	*CR*	*C*	5.5 h	172.2	32.33	18
^{112}Pd	1.76 ± 0.03	*CR*	*C*	21.05 h	617.4[f]	50.0	19
^{103}Ag	0.267 ± 0.088	*CD*	*C*	1.095 h	118.7	31.3	19
^{104}Ag^m	0.600 ± 0.393	*I*	*C*	33.5 min	767.6[f]	65.78	18
^{104}Ag^g	< 0.51[c]	*I*	*C*	69.2 min	767.6	65.78	18
^{105}Ag	4.21 ± 0.15	*CD*	*C*	41.0 d	344.4	42.	17
^{106}Ag^m	6.43 ± 0.08	*I*	*C*	8.410 d	1045.7	29.7	17
^{110}Ag^m	23.7 ± 0.6	*I*	*C*	253. d	657.7	93.8	17
^{111}Ag	24.9 ± 2.6	*I*[d]	*C*	7.47 d	342.1	6.7	19
^{112}Ag	13.8 ± 0.4	*I*	*C*	3.14 h	617.4	42.	18
^{113}Ag	12.8 ± 0.4	*CR*	*C*	5.299 h	298.4	8.2	17
^{107}Cd	1.53 ± 0.55	*CD*	*C*	6.499 h	93.1	4.6	17
^{111}Cd^m	18.1 ± 1.2	*I*	*C,D*	46.8 min	245.4	94.	17
^{115}Cd^g	1.42 ± 0.48	*CR*	*C*	2.221 d	527.9	27.5	17
^{109}In	1.16 ± 0.41	*CD*	*C*	4.301 h	203.5	72.1	17
^{110}In^B	2.64 ± 0.59	*I*	*C,D*	4.901 h	884.7	94.9	17
^{111}In	6.85 ± 2.38	*CD*	*C*	2.83 d	171.3	90.3	17
^{114}In^m	21.4 ± 7.5	*I*	*C*	49.5 d	558.3	3.40	19
^{116}In^m	13.8 ± 4.8	*I*	*C,D*	54.101 min	1293.4	85.	17
^{115}Sb	5.64 ± 1.06	*CD*	*C*	31.8 min	498.	99.1	18
^{116}Sb^m	4.26 ± 0.86	*I*	*C,D*	1.005 h	972.6	72.	17
^{116}Sb^g	3.13 ± 0.99	*I*	*D*	15.998 min	1293.7	88.	17
^{118}Sb^m	9.87 ± 0.43	*I*	*C,D*	5.1 h	253.5	99.	18
^{120}Sb^B	6.66 ± 0.42	*I*	*C,D*	5.76 d	1171.7	100.	18
^{122}Sb	4.73 ± 0.38	*I*	*C*	2.681 d	564.1	70.	18
^{116}Te	1.27 ± 0.11	*CD*	*C,D*	2.50 h	94.1	29.	18
^{117}Te	< 0.19[c]	*CD*	*C*	61. min	719.7	65.	18
^{118}Te	7.99 ± 2.49	*I*	*C*	6.0 d	1229.5[f]	2.5	18
^{119}Te^m	5.83 ± 0.38	*I*	*C*	4.68 d	153.5	66.	18
^{119}Te^g	1.93 ± 0.17	*I*	*C*	16.05 h	644.01	84.	18
^{121}Te^m	10.5 ± 1.4	*I*	*C*	154. d	212.2	83.	18
^{121}Te^g	1.83 ± 0.39	*I*	*C,D*	16.78 d	573.01	80.3	18
^{123}Te^m	6.51 ± 0.25	*I*	*C*	119.7 d	159.	83.6	18
^{118}I	1.79 ± 0.48	*CD*	*C*	14.3 min	605.2	95.	18
^{119}I	0.568 ± 0.242	*CD*	*C*	19.296 min	257.6	95.	17
^{120}I^B	0.611 ± 0.153	*I*	*C*	53. min	560.4	100.	18
^{120}I^A	1.05 ± 0.23	*CD*	*C*	1.35 h	560.4	73.	18
^{121}I	4.14 ± 0.29	*CD*	*C,D*	2.12 h	212.5	84.3	17
^{123}I	9.31 ± 0.77	*CD*	*C,D*	13.099 h	159.1	83.	17
^{124}I	6.39 ± 0.78	*I*	*C*	4.17 d	602.7	62.	17
^{126}I	3.37 ± 0.75	*I*	*C*	13.0 d	388.6	34.9	17
^{130}I	0.542 ± 0.117	*I*	*C*	12.36 h	668.4	94.	18
^{127}Xe	12.6 ± 1.7	*CD*	*D*	36.4 d	202.8	68.3	19
^{129}Cs	4.64 ± 0.65	*CD*	*C*	33.35 h	371.9	32.	18
^{132}Cs	0.683 ± 0.083	*I*	*C*	6.474 d	667.5	97.5	18
^{126}Ba	2.55 ± 0.50	*CD*	*C*	100. min	388.6[f]	42.	18
^{128}Ba	1.61 ± 0.45	*CD*	*C*	2.43 d	443.[f]	25.8	18
^{131}Ba^m	2.19 ± 2.04	*I*	*C,D*	14.60 min	107.	56.	18
^{131}Ba^g	4.90 ± 0.95	*CD*	*C,D*	12.0 d	123.7	28.	18

TABLE I. (*Continued*).

Nuclide	Cross section (mb)	Type[a]	Method[b]	Half-life	E_γ (keV)	I_γ (%)	Reference
$^{133}Ba^m$	1.08 ± 0.34	*I*	*C*	38.9 h	275.6	17.5	18
^{130}La	0.797 ± 0.465	*I*	*C*	8.7 min	357.3	81.	18
^{131}La	1.81 ± 0.97	*CD*	*C*	61. min	108.1	24.	18
$^{132}La^m$	4.60 ± 3.10	*I*	*D*	24.307 min	135.8	43.0	18
$^{132}La^g$	2.02 ± 0.54	*I*	*C*	4.8 h	464.55	76.	18
^{134}La	4.42 ± 1.95	*I*	*C*	6.67 min	604.7	5.04	18
^{136}La	4.83 ± 2.23	*I*	*C*	9.87 min	818.51	2.6	18
^{130}Ce	0.163 ± 0.157	*CD*	*C*	25. min	357.3[f]	81.	18
$^{131}Ce^A$	2.90 ± 0.92	*CD*	*C*	10.5 min	169.6	20.	18
^{132}Ce	0.824 ± 0.160	*CD*	*C*	3.51 h	464.55[f]	76.	18
$^{133}Ce^g$	1.12 ± 0.20	*CD*	*C*	4.9 h	130.7	17.9	19
^{134}Ce	1.59 ± 1.19	*CD*	*C*	75.9 h	604.7[f]	5.04	18
^{135}Ce	3.03 ± 0.55	*CD*	*C*	17.6 h	265.3	46.	17
$^{137}Ce^m$	1.29 ± 0.05	*I*	*C*	34.4 h	254.3	11.1	18
$^{137}Ce^g$	2.92 ± 0.96	*CD*	*C*	9.0 d	447.15	2.2	18
^{139}Ce	3.16 ± 0.57	*CD*	*C*	137.2 d	165.9	80.	18
^{141}Ce	0.038 ± 0.011	*CR*	*C*	32.55 d	145.4	49.3	18
^{136}Pr	0.927 ± 0.146	*I*	*C*	13.1 min	539.8	52.4	18
$^{138}Pr^m$	1.44 ± 0.43	*I*	*C*	2.02 h	789.0	100.	18
^{136}Nd	0.451 ± 0.114	*CD*	*C*	50.65 min	574.9	12.	18
^{137}Nd	0.571 ± 0.141	*CD*	*C*	38.5 min	580.6	13.	18
^{138}Nd	2.02 ± 1.20	*CD*	*C*	5.04 h	326.3	2.9	18
$^{139}Nd^m$	1.01 ± 0.05	*I*	*C*	5.5 h	113.9	34.0	19
$^{140}Pm^m$	0.269 ± 0.125	*I*	*C*	5.95 min	419.9	91.63	18
^{141}Pm	2.20 ± 0.82	*CD*	*C*	20.9 min	1223.26	4.6	19
^{144}Pm	0.803 ± 0.665	*I*	*C*	349. d	696.5	100.	18
$^{141}Sm^g$	0.300 ± 0.090	*CD*	*C*	10.2 min	403.9	42.4	18
$^{141}Sm^m$	0.192 ± 0.054	*CD*	*C*	22.5 min	196.6	73.6	18
^{142}Sm	0.269 ± 0.114	*CD*	*C*	72.49 min	1576.[f]	3.0	18
^{145}Eu	0.398 ± 0.071	*CD*	*C*	5.93 d	893.5	65.	18
^{146}Eu	0.429 ± 0.102	*I*	*C*	4.7 d	747.2	97.8	17
^{147}Eu	0.770 ± 0.173	*I*	*C*	24.3 d	197.3	23.	17
^{148}Eu	0.286 ± 0.010	*I*	*C*	54. d	550.2	99.	18
^{145}Gd	0.200 ± 0.070	*CD*	*C*	21.8 min	1757.8	35.	18
^{146}Gd	0.079 ± 0.025	*CD*	*C*	48.3 d	115.3	45.	17
^{147}Gd	0.253 ± 0.060	*CD*	*C*	1.458 d	229.3	64.4	19
^{149}Gd	0.549 ± 0.027	*CD*	*C*	9.25 d	149.7	41.7	19
$^{147}Tb^A$	0.123 ± 0.049	*CD*	*C*	1.61 h	1153.	75.	18
^{151}Tb	0.329 ± 0.157	*CD*	*C*	17.6 h	108.1	25.22	18
^{152}Tb	0.271 ± 0.024	*I*	*C*	17.5 h	344.3	57.	19
^{153}Tb	0.506 ± 0.033	*I*	*C*	2.34 d	211.94	32.5	19
^{155}Tb	0.376 ± 0.066	*CD*	*C*	5.32 d	105.3	23.	18
^{156}Tb	0.049 ± 0.010	*I*	*C*	5.35 d	534.3	67.0	18
^{152}Dy	0.215 ± 0.040	*CD*	*C*	2.37 h	257.	97.6	18
^{153}Dy	0.526 ± 0.059	*CD*	*C*	6.50 h	254.3	8.33	19
^{155}Dy	0.332 ± 0.063	*CD*	*C*	10. h	227.	68.	18
^{157}Dy	0.337 ± 0.063	*CD*	*C*	8.1 h	326.3	95.0	17
^{156}Ho	0.617 ± 0.094	*CD*	*C*	55.6 min	266.4	53.9	19
^{160}Er	0.214 ± 0.085	*CD*	*C*	1.225 d	728.1[f]	36.	19
^{161}Er	0.225 ± 0.045	*CD*	*C*	3.24 h	826.5	61.	18
^{167}Tm	0.114 ± 0.087	*CD*	*C*	9.25 d	207.8	41.0	18
^{166}Yb	0.167 ± 0.095	*CD*	*C*	56.7 h	184.3[f]	21.3	19
^{167}Yb	0.086 ± 0.073	*I*	*C*	17.7 min	113.32	54.	18
^{169}Lu	0.142 ± 0.059	*CD*	*C*	34.06 h	191.2	17.9	19
^{170}Hf	< 0.05[c]	*CD*	*C*	15.92 h	164.78	33.	18
^{173}Hf	0.110 ± 0.007	*I*	*C*	24.0 h	123.69	83.	18
^{173}Ta	0.064 ± 0.004	*CD*	*C*	3.701 h	123.69[f]	83.	18
^{174}Ta	0.057 ± 0.057	*CD*	*C*	1.2 h	206.5	66.2	17
^{175}Ta	0.164 ± 0.017	*CD*	*C*	10.5 h	207.4	13.3	17

TABLE I. (*Continued*).

Nuclide	Cross section (mb)	Type[a]	Method[b]	Half-life	E_γ (keV)	I_γ (%)	Reference
^{176}Ta	0.197 ± 0.028	*CD*	*C*	8.1 h	1159.3	24.0	17
^{177}Ta	0.192 ± 0.025	*CD*	*C*	2.358 h	113.0	6.0	17
^{178}Ta^{m}	0.014 ± 0.005	*I*	*C*	2.45 h	325.6	94.1	18
^{176}W	0.150 ± 0.010	*CD*	*C*	2.3 h	100.2	71.	17
^{177}W	0.104 ± 0.010	*CD*	*C*	2.25 h	115.7	58.5	19
^{178}W	0.680 ± 0.623	*CD*	*C*	21.5 d	1350.6[f]	1.17	18
^{180}Os	0.331 ± 0.103	*CD*	*C*	21.7 min	902.4[f]	98.	18
^{181}Os^{B}	0.107 ± 0.008	*CD*	*C*	105. min	238.7	46.2	18
^{182}Os	1.12 ± 0.08	*CD*	*C*	22.10 h	180.2	33.2	18
^{183}Os^{m}	0.864 ± 0.044	*CD*	*C*	9.9 h	1102.	55.	18
^{183}Os^{g}	0.625 ± 0.039	*CD*	*C*	13. h	114.4	19.8	18
^{185}Os	1.37 ± 0.19	*CD*	*C*	93.6 d	646.07	81.	18
^{184}Ir	< 3.5[c]	*CD*	*D*	3.101 h	119.8	33.2	17
^{186}Ir^{A}	< 4.4[c]	*I*	*D*	1.75 h	630.3	19.3	17
^{188}Ir	6.83 ± 1.22	*I*	*C*	1.729[d]	663.1	22.	17
^{186}Pt	2.15 ± 0.07	*CD*	*C*	2.0 h	434.8[f]	33.7	18
^{187}Pt	5.17 ± 0.27	*CD*	*C*	2.35 h	201.5	7.6	17
^{188}Pt	19.0 ± 0.5	*CD*	*C*	10.2 d	187.6	19.2	18
^{189}Pt	34.5 ± 0.6	*CD*	*C,D*	10.87 h	243.5	4.4	18
^{191}Pt	9.03 ± 0.22	*I*	*C*	3.0 d	409.4	7.9	17
^{197}Pt	1.88 ± 0.11	*CR*	*C*	18.3 h	191.4	3.485	18
^{189}Au	11.1 ± 2.7	*CD*	*C*	28.7 min	721.4[f]	5.8	18
^{190}Au	11.7 ± 1.0	*I*	*C*	42.8 min	296.0	71.	18
^{191}Au	13.3 ± 0.7	*I*	*C*	3.199 h	586.4	16.0	19
^{192}Au	9.10 ± 0.87	*I*	*C*	5.03 h	316.6	78.3	19
^{193}Au	10.5 ± 1.8	*I*[e]	*C*	17.5 h	255.6	7.	18
^{194}Au	32.9 ± 2.5	*I*	*C,D*	39.5 h	328.47	61.	18
^{196}Au^{m}	5.80 ± 0.38	*I*	*C,D*	9.701 h	147.7	42.0	17
^{196}Au^{g}	139. ± 7.	*I*	*C,D*	6.18 d	355.7	88.0	17
^{198}Au^{m}	1.23 ± 0.14	*I*	*C*	2.27 d	214.9	78.7	17
^{198}Au^{g}	17.9 ± 0.9	*I*	*C*	2.69 d	411.8	94.7	17
^{199}Au	0.794 ± 0.122	*CR*	*C*	3.148 min	158.24	39.	18
^{190}Hg	36.2 ± 1.5	*CD*	*D*	20.00 min	142.7	52.0	19
^{191}Hg	26.7 ± 1.5	*CD*	*C*	50.8 min	252.6	55.1	17
^{192}Hg	23.5 ± 4.7	*I*	*C*	4.901 h	274.8	46.1	17
^{193}Hg^{m}	17.9 ± 1.0	*I*	*C,D*	11.8 h	407.7	37.0	19
^{195}Hg^{m}	29.9 ± 5.5	*I*	*C,D*	1.667 d	261.8	33.4	19
^{197}Hg^{m}	28.7 ± 5.4	*I*	*C*	23.8 h	133.9	34.3	18
^{197}Hg^{g}	3.13 ± 1.53	*I*	*C*	64.14 h	77.35	19.	18
^{199}Hg^{m}	8.63 ± 0.85	*I*	*D*	42.595 min	158.4	58.4	17
^{192}Tl	35.1 ± 9.2	*CD*	*C,D*	10.7 min	274.8[f]	46.1	17
^{193}Tl	45.8 ±12.6	*CD*	*C*	21. min	255.6[g]	7.	18
^{194}Tl^{m}	38.7 ± 3.4	*I*	*C,D*	32.8 min	748.9	77.	18
^{194}Tl^{g}	33.2 ±11.9	*CD*	*C,D*	35.107 min	645.5	13.0	17
^{195}Tl	71.3 ± 4.5	*I*	*C*	1.16 h	884.5	10.5	19
^{196}Tl^{m}	88.0 ± 5.1	*I*	*C*	1.410 h	426.3	92.	17
^{196}Tl^{g}	5.63 ± 1.56	*I*	*C*	1.90 h	610.6	12.4	17
^{197}Tl	64.1 ± 4.5	*I*	*C*	2.837 h	307.8+308.6	3.6	19
^{198}Tl^{m}	16.3 ± 1.5	*I*	*C*	1.870 h	282.8	27.	17
^{198}Tl^{g}	9.81 ± 1.27	*I*	*C*	5.3 h	1420.6	8.0	17
^{199}Tl	4.49 ± 1.05	*I*	*C*	7.399 h	455.1	13.6	17
^{200}Tl	0.324 ± 0.006	*I*	*C*	1.088 d	368.0	91.0	17
^{201}Tl	0.070 ± 0.009	*I*	*C*	73. h	167.4	10.6	19
^{202}Tl	0.030 ± 0.013	*I*	*C*	12.2 d	439.4	94.	17
^{195}Pb^{g}	27.3 ± 6.4	*CD*	*D*	17.006 min	383.5	93.5	17
^{196}Pb	30.0 ± 3.4	*CD*	*C*	36.994 min	425.7[f]	87.2	17
^{197}Pb^{m}	23.3 ± 1.6	*CD*	*C*	42.005 min	385.6	77.2	17
^{198}Pb	12.6 ± 2.7	*I*	*C*	2.4 h	365.4	19.	19
^{199}Pb	5.74 ± 1.23	*CD*	*C,D*	1.5 h	366.9	64.8	19

TABLE I. (*Continued*).

Nuclide	Cross section (mb)	Type[a]	Method[b]	Half-life	E_γ (keV)	I_γ (%)	Reference
^{200}Pb	0.983 ± 0.182	*I*	*C*	21.499 h	147.6	37.7	19
^{201}Pb	0.252 ± 0.013	*I*	*C*	9.401 h	331.2	81.4	17
$^{202}Pb^m$	0.085 ± 0.035	*I*	*C*	3.619 h	960.7	91.3	17
^{203}Pb	0.006 ± 0.002	*I*	*C*	2.171 d	279.2	81.0	17
^{198}Bi	6.29 ± 0.49	*CD*	*D*	11.85 min	1063.5	100.	17
$^{200}Bi^g$	0.623 ± 0.143	*CD*	*C*	36.4 min	1026.	100.	18
^{201}Bi	0.127 ± 0.005	*CD*	*C*	1.8 h	331.2[f]	81.4	17
^{202}Bi	0.030 ± 0.012	*I*	*C*	1.67 h	961.	100.	18
^{203}Bi	0.016 ± 0.012	*CD*	*C*	11.8 h	820.	29.	18
^{204}Bi	0.005 ± 0.002	*I*	*C*	11.2 h	899.	100.	18
^{198}Po	0.780 ± 0.100	*I*	*RC*	1.78 min	α (6.183	70.)[h]	18
$^{199}Po^m$	0.183 ± 0.037	*I*	*RC*	4.2 min	α (6.060	39.)[h]	18
^{200}Po	0.089 ± 0.020	*I*	*RC*	11.6 min	α (5.864	14.)[h]	18
^{202}Po	0.034 ± 0.012	*CD*	*C*	44. min	686.9	47.	18
^{204}Po	0.028 ± 0.021	*CD*	*C*	3.52 h	1016.1	24.4	19

[a] *I*: Independent; *CD*: Partially cumulative from EC or β^+; *CR*: Partially cumulative from β^-.
[b] *C*: Chemically separated; *D*: Nondestructive, *RC*: Rapid chemistry for α counting.
[c]Peak was observed, but large error.
[d]Not corrected for $^{111}Pd^g$.
[e]$^{193}Hg^m/^{193}Hg^g = 3$ was assumed.
[f]Obtained from daughter nuclide.
[g]Obtained from granddaughter nuclide.
[h]Alpha energy in MeV.

The full width at half maximum is about 38, which is larger than those for the 126 MeV ^{14}N induced fission of ^{197}Au (FWHM=30±2),[23] the 112 MeV ^{12}C induced fission of ^{197}Au (FWHM=27),[20] and the 105 MeV ^{12}C induced fission of ^{196}Pt (FWHM=29.2),[24] but is smaller than that for the reaction products from 391 MeV $^{40}Ar+^{165}Ho$ (FWHM=60) (Ref. 25) for which it is assumed that there is a contribution due to other reaction processes. If we assume that the charge distributions of the fission products are the same as those of the fissioning nuclei, ignoring the possibility of neutron emission from the fission fragments, the "average" fissioning nucleus is near ^{191}Tl.

Blann[20] has measured a fission cross section of 0.9 b in the reaction of 112 MeV ^{12}C with ^{197}Au. Gordon *et al.*[27] gave 1.28 b for the fission cross section in the reaction of 124 MeV ^{12}C with ^{197}Au, and Britt and Quinton[28] gave 1.35 b for 126 MeV $^{12}C+^{197}Au$. Wilcke *et al.*[26] have calculated fusion cross sections for the $^{12}C+^{197}Au$ system at a variety of energies. For each of the reactions listed previously, the calculated fusion cross section is larger than the observed fission cross section. The calculated fusion cross section in the 20 MeV/nucleon $^{12}C+^{197}Au$ system is 967 mb. From the fit to the charge-dispersion-corrected mass yield, shown in Fig. 1(b), we obtain a fission cross section of 1700 mb. In this case there are two significant contributions to the fission cross section: fusion-fission and fission following multinucleon transfer (sequential fission). As a simplest case, if a single proton with the velocity of the ^{12}C projectile is deposited in a ^{197}Au nucleus to make $^{198}Hg^*$, the excitation energy of the ^{198}Hg is about 27 MeV. The fission barrier of ^{198}Hg is on the same order,[29] about 22 MeV. From $^{197}Au(p,f)$ data[30] it is known that the contribution to the fission cross section from ^{198}Hg precursors is small at these excitation energies; however, the transfer of more nucleons to the target nuclei and the possibility of damping some of the relative motion of the reacting system into excitation energy and intrinsic angular momentum makes it possible to attribute the "extra" 700 mb of fission cross section to sequential fission processes.

When the evaporation code ALICE,[31] including preequilibrium processes, was used to model the reaction of 240 MeV $^{12}C+^{197}Au$, the resultant fission cross section was 1700 mb. The initial exciton number was varied from 12 to 20, but this did not greatly affect the value of the fission cross section. This is a not unexpected result since, generally, fission occurs at rather low excitation energies, after several nucleon emissions in this case. Gordon *et al.*[27] measured the angular distributions of fission fragments in the $^{12}C+^{197}Au$ system at different incident projectile energies. They concluded that the average excitation energy of the fissioning nuclei is independent of projectile energy. At high excitation, fast processes like particle emission dominate; the slower fission process cannot compete until the excitation energy has been decreased to about 25 MeV. We do not consider the possibility of "fast fission" processes since, in the reaction of 20 MeV/nucleon ^{12}C with ^{197}Au, the critical angular momentum of fusion is $20\hbar$ smaller than the value of the angular momentum at which the fission barrier of the compound nucleus vanishes.[26]

The determination of isomer ratios gives a rough measure of the energy and angular momentum in the precur-

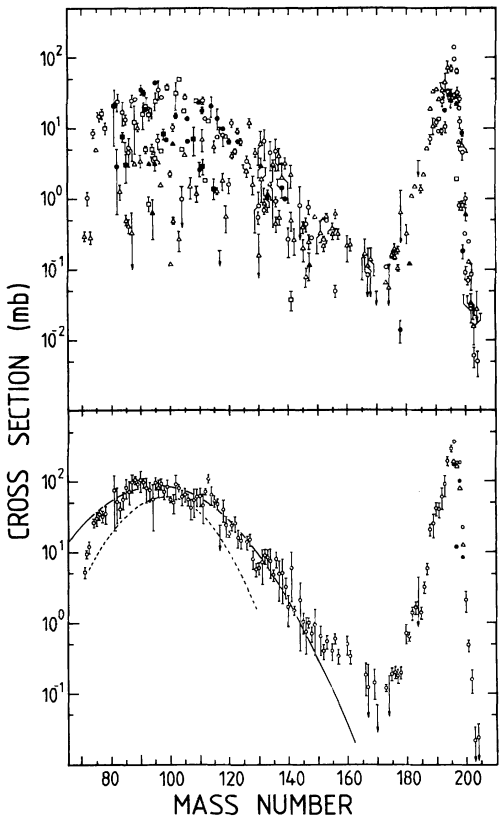

FIG. 1. Cross sections from the reaction of 240 MeV ^{12}C with ^{197}Au. (a) (Upper). Individual cross sections. Circles denote independent cross sections, triangles denote partially cumulative cross sections from β^+ or EC decay, and squares denote partially cumulative cross sections from β^- decay. Solid points denote the cross section for one member of an isomer pair. (b) (Lower). The charge-dispersion-corrected mass distribution. The meanings of symbols other than circles for targetlike products are described in the text. The full curve is a result of Gaussian fitting the fission products, and the dashed curve is that from Ref. 20 describing the fission distribution of 112 MeV $^{12}C+^{197}Au$.

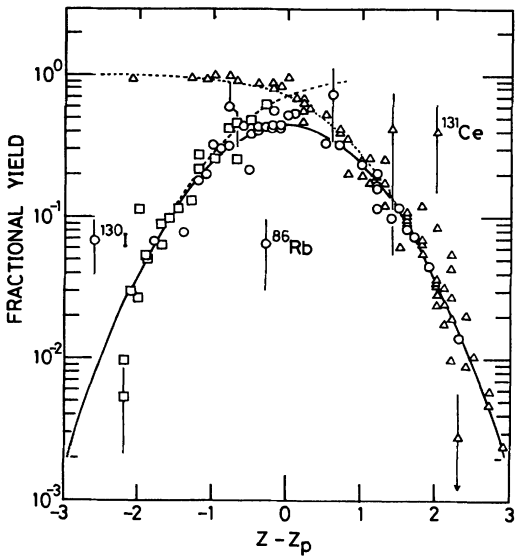

FIG. 2. The cumulative charge dispersion of the fission products. Circles denote independent cross sections, triangles denote partially cumulative cross sections from β^+ or EC decay, and squares denote partially cumulative cross sections from β^- decay.

sor nuclides. The isomer ratios measured in this work are tabulated in Table II, together with the isomer ratios for the same nuclides determined in other reactions.[32–37] The isomer ratio of ^{85}Sr is significantly higher in our work than that arising from $^{84}Sr(n_{th},\gamma)$ reactions,[32] indicating that the precursor resulting in ^{85}Sr has a nonzero angular momentum.[38] The isomer ratios of ^{116}Sn and ^{119}Te in the present work are very nearly equal to those obtained from the complete fusion reactions $^{115}In(\alpha,3n)$ and $^{118}Sn(\alpha,3n)$ at $E_\alpha=33$ MeV.[34] The isomer ratio we have determined for ^{121}Te is only somewhat larger than that from $^{120}Sn(\alpha,3n)$ at $E_\alpha=33$ MeV.[34] Reference 34 gives an isomer ratio for ^{126}Sb from the $^{124}Sn(\alpha,pn)$ reaction at $E_\alpha=36.5$ MeV which is similar to the $(\alpha,3n)$ values given above. However, the isomer ratio of ^{126}Sb produced in the reaction of 94 MeV ^{12}C with ^{209}Bi,[39] which proceeds largely via a complete fusion mechanism, is about 2.5 times larger than that from the $^{124}Sn(\alpha,pn)$ reaction. The small values of the isomer ratios for the fission products obtained in our experiments is another indication that much of the fission cross section arises from relatively low angular momentum sequential fission processes rather than from the high angular momentum complete fusion process.

B. Targetlike products

The cross sections of targetlike reaction products are plotted in Fig. 1 with the cross sections of the fission products. As shown in Fig. 3, the charge dispersions of $A=200$ to 204 can be fit with single Gaussian distributions with width parameters $(2\sigma^2)$ of about 1.6. For $A=196$ to 199, the charge dispersions seem to have two components. The high-Z nuclides can be described with a width parameter of 1.1, while the low-Z peaks are much narrower, with $2\sigma^2=0.6$. The most probable charge associated with the small width parameter increases with mass number, consistent with a quasielastic reaction mechanism where the reaction products are centered about the (Z,A) of the target. The more neutron deficient products described with the larger width parameter are due to some combination of complete fusion, deep-inelastic, and/or several-nucleon-transfer processes. The most probable charge of these products remains constant at $Z=82$ for nuclei with $A=198$ to 202. This is due, in part, to the effect of the $Z=82$ shell on the transfer process and on its effect on the fission survival probability of the primary reaction products.

The ALICE calculation described earlier did not reproduce the cross sections of most of the targetlike products. The systematic behavior of the calculated cross sections was contrary to that observed in the experiment, with cross sections falling off from the compound nucleus (Z,A). The experimental cross sections of the Tl, Pb, and Bi isotopes are one to two orders of magnitude larger than the calculated cross sections. The calculation did repro-

TABLE II. Isomer ratios ($\sigma_{\text{high spin}}/\sigma_{\text{low spin}}$) from the reaction of 240 MeV ^{12}C with ^{197}Au.

Nuclide	Spins	$\frac{\sigma_h}{\sigma_l}$, present work	$\frac{\sigma_h}{\sigma_l}$, other reactions	
^{84}Rb	(6+),2−	4.4 ±2.5		
^{85}Sr	$\frac{9}{2}+,\frac{1}{2}-$	28 ±9	0.67[a]	(n_{th},γ')
^{86}Y	8+,4−	0.66 ±0.59	0.45[b]	$(p,3n),E_p=660$ MeV
^{116}Sb	8−,3+	1.4 ±0.6	2.03 ±0.10[c]	$(\alpha,3n),E_\alpha=32.3$ MeV
^{119}Te	$\frac{11}{2}-,\frac{1}{2}+$	3.0 ±0.8	2.70 ±0.05[c]	$(\alpha,3n),E_\alpha=33.4$ MeV
^{121}Te	$\frac{11}{2}-,\frac{1}{2}+$	5.7 ±2.1	2.00 ±0.30[c]	$(\alpha,3n),E_\alpha=33.4$ MeV
^{132}La	6−,2−	2.3 ±1.9		
^{160}Ho	5+,2−	0.87 ±0.70		
^{196}Au	12−, (2− and 5^+)	0.042±0.011	0.054±0.004[d]	$(n,2n),E_n=13.4$ MeV
^{198}Au	(12−),2−	0.069±0.023		
^{197}Hg	$\frac{13}{2}+,\frac{1}{2}-$	9.2 ±4.8	1.04 ±0.15[e]	$(d,2n),E_d=21.4$ MeV
^{196}Tl	(7+),2(−)	15.6 ±4.4		
^{198}Tl	7+,2−	1.66 ±0.50	12[f]	$(\alpha,3n),E_\alpha=35$ MeV

[a]Reference 32.
[b]Reference 33.
[c]Reference 34.
[d]Reference 35.
[e]Reference 36.
[f]Reference 37.

duce the cross sections of the polonium isotopes, except for ^{202}Po and ^{204}Po. This, and the shift of the charge distributions away from $Z_p=82$ for $A=203$ and 204, we attribute to the deexcitation of primary products near the (Z,A) of the compound nucleus by the emission of nonequilibrium high energy nucleons.

In Fig. 4, the cross sections of the Tl, Pb, Bi, and Po isotopes are plotted versus the Q_{gg} for their formation via

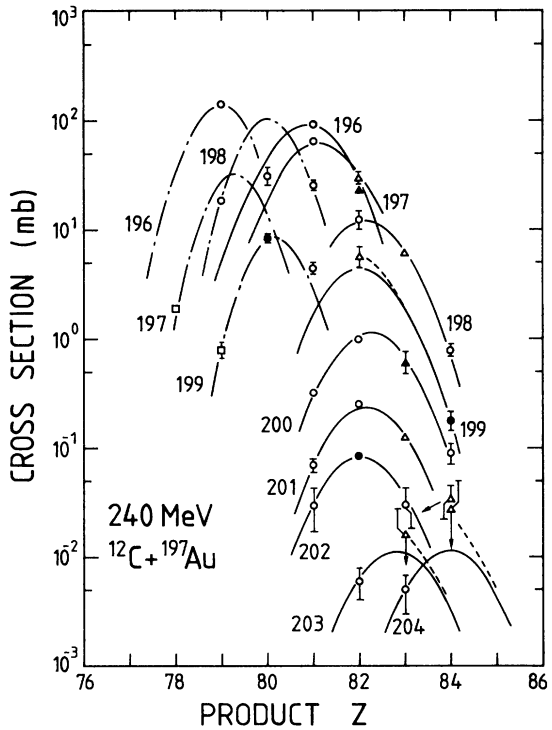

FIG. 3. The charge dispersions of targetlike products for $A=196$ to 204. Circles denote independent cross sections, triangles denote partially cumulative cross sections from β^+ or EC decay, and squares denote partially cumulative cross sections from β^- decay. Solid points denote the cross section for one member of an isomer pair.

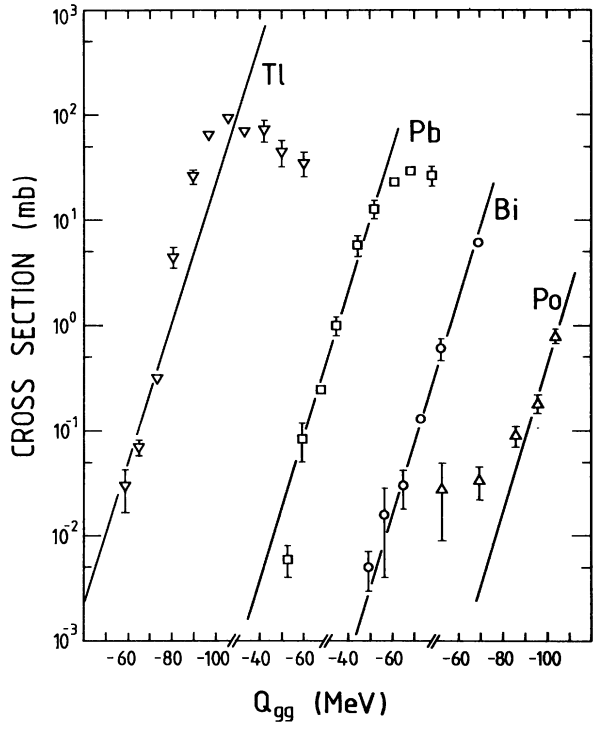

FIG. 4. The dependence of the isotopic distribution of high Z products on Q_{gg}. The calculation of Q_{gg} in this case is discussed in the text. Circles denote independent cross sections, triangles denote partially cumulative cross sections from β^+ or EC decay, and squares denote partially cumulative cross sections from β^- decay.

a "compound nucleus." Volkov[40] has used the Q_{gg} method to extract the nuclear temperature of partial fusion reactions from projectilelike reaction products, assuming a binary reaction mechanism. Jacmart *et al.*[41] were not able to reproduce a similar systematic Q_{gg} dependence. Here, the ^{12}C projectile is so small that we assume that the complementary fragment for the production of species at a significantly higher Z than the target nucleus exists as a set of discrete, unbound nucleons. We have, in effect, assumed for the purpose of the Q_{gg} calculation that the polonium isotopes are produced in $^{197}Au(^{12}C,pxn)$ reactions, that the bismuth isotopes are produced in $^{197}Au(^{12}C,2pxn)$ reactions, etc. Since the binding energy of the neutron is positive for all the targetlike products, the mass numbers of the isotopes of a given element decrease from left to right in Fig. 4. The solid lines are drawn parallel to the linear fit to the bismuth data. The strongest deviations from linear behavior occur in the thallium isotopes, where the size of the complementary fragments ($_4$Be) for the more neutron deficient products makes the discrete-nucleon assumption untenable. Since we are plotting evaporation residue cross sections rather than the cross sections of primary products, the slope no longer directly relates to the reaction temperature; in fact, the slope is of the opposite sign from that obtained by Volkov.[40]

The charge-corrected mass distribution of targetlike products is shown in Fig. 1(b) along with that of the fission products. In the case of $A=196$ to 199, the quasielastic component (closed circles) and the deep-inelastic component (triangles) were integrated separately, then summed to give the data plotted as open circles. The total cross section for the production of targetlike products ($A=170$ to 204) is about 1600 mb. Combined with the fission cross section of 1700 mb, this gives a total reaction cross section of about 3.3 b, in excellent agreement with the value calculated by Wilcke *et al.*[26] of 3.3 b.

The isotopic distributions for $Z=78$ to 84 are plotted in Fig. 5. In general, there is a downward trend in the maximum cross section of each element distribution as the nuclear charges of the products increase from the target Z. The apparent exception for the mercury isotopes ($Z+1$) is due to the fact that the observed cross sections near the predicted maximum are for only one-half of an isomer pair. The cross sections of the thallium ($Z+2$) and bismuth ($Z+4$) isotopes are much lower than those arising from the $^{12}C+^{197}Au$ reaction at lower projectile energies.[42]

The isomeric yield ratios of targetlike products are tabulated in Table II. The ^{160}Ho isomer ratio arises from the decay curve analysis of the gamma rays of $^{160}Ho^g$, given the internal transition branch of 65%.[18] Due to the angular momentum dependence of the competition of fission to particle evaporation, the obtained isomer ratios do not directly relate to the angular momentum of the composite system or the spin distribution in the primary reaction products. They do give some indication of the reaction mechanism resulting in these evaporation residues. The cross section ratio of high spin to low spin isomers in ^{198}Tl, ^{196}Tl, and ^{197}Hg are all larger than those for the typical quasielastic products ^{196}Au and ^{198}Au. Even at these

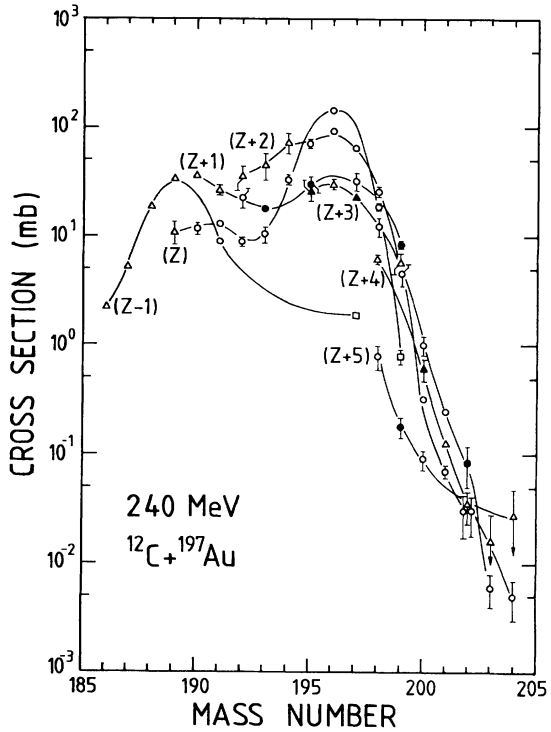

FIG. 5. The isotopic distributions of targetlike products. Z refers to the atomic number of the target nucleus (79). Circles denote independent cross sections, triangles denote partially cumulative cross sections from β^+ or EC decay, and squares denote partially cumulative cross sections from β^- decay. Solid points denote the cross section for one member of an isomer pair.

projectile energies, the "thermalization" of angular momentum in the quasielastic channels is very small, on the order of that introduced by 13 MeV neutrons in the $^{197}Au(n,2n)$ reaction. The relative sizes of the ^{198}Tl and ^{196}Tl isomer ratios we cannot explain.

IV. CONCLUSION

The cross sections of about 250 nuclides were measured in the reaction of 20 MeV/nucleon ^{12}C with ^{197}Au. The charge dispersion of fission products had a Gaussian shape with a width parameter ($2\sigma^2$) of 1.6, which is larger than those obtained from lower energy systems. The FWHM of the mass yield curve of the fission products was 38 mass units, and the fission cross section was about 1.7 b. Both these values are larger than those obtained in low energy heavy-ion-induced fission. The broadening of the charge dispersion and mass distribution of the fission products may be attributed to the large variety of the fissioning nuclei of high angular momentum. The isomer ratios of the fission products were similar to those measured in low energy charge-particle-induced reactions.

The charge dispersions of $A=196$ to 199 seem to have two components, one corresponding to quasielastic processes, and the other corresponding to deep-inelastic and/or complete fusion processes. The peak cross sections of the transtarget elements decrease with increasing

Z, contrary to the result expected from an evaporation calculation. The summed cross section of targetlike products was about 1.6 b. The total reaction cross section was approximately 3.3 b, which is in agreement with the theoretical estimate of 3.3 b.

ACKNOWLEDGMENTS

The authors would like to thank the staff and crew of the 88-Inch Cyclotron for their assistance and support. We would also like to thank Professor W. Loveland for his interest and Dr. Y. Morita for his help with irradiations. One of us (H.K.) would like to thank the Lawrence Berkeley Laboratory for a pleasant stay and is indebted to the members of the LBL-INS collaboration group. The continuous encouragement of Professor H. Nakahara is gratefully acknowledged. This work was supported by the U.S. Department of Energy under Contract No. DE-AC03-76SF00098.

APPENDIX

The following are notes on the chemical procedures used to separate the elements near gold from the fission products and from each other.

Hafnium: After separation from the lanthanides, hafnium was coprecipitated with barium fluorozirconate. The precipitate was dissolved in boric acid and nitric acid, and a hydroxide precipitation was performed by adding ammonium hydroxide. The precipitate was dissolved in a small amount of hydrochloric acid, and loaded on an anion exchange column (Dowex AG 1-X8). Hafnium was eluted with a $4N$-HCl—$0.1N$-HF solution.

Tantalum: Tantalum oxide was precipitated from fuming HNO_3. The precipitate was washed with NH_4OH to remove tungsten (see the following), and then tantalum was dissolved in hydrofluoric acid. Lanthanum hydroxide, antimony sulfide, and barium fluorozirconate scavenge procedures were performed. Tantalum oxide was reprecipitated by adding boric acid in a nitric acid solution.

Tungsten: Tungsten was precipitated from fuming HNO_3. After dissolving in NH_4OH and scavenging with $Fe(OH)_3$, tungsten was precipitated with 8-hydroxyquinoline in an ammonium acetate-acetic acid buffer solution.

Rhenium: Rhenium was distilled from concentrated H_2SO_4 into a NaOH solution. After scavenging with $Fe(OH)_3$ and $Ru(OH)_3$ precipitations, rhenium was precipitated with tetraphenyl arsonium. In this work, however, we could not measure the gamma rays of any rhenium isotopes, probably due to their small cross sections and the low chemical yield of this procedure.

Osmium: Osmium was distilled from concentrated HNO_3 into $6N$ NaOH, and precipitated with hydrogen sulfide with the addition of hydrochloric acid.

Iridium: After separation from platinum with an ethyl acetate extraction, iridium was reduced to the metallic state with formic acid.

Platinum: Initially, gold and thallium contaminants were extracted from a $3N$ HCl solution with ethyl acetate (see the following). Then platinum(IV) was reduced to platinum(II) with Sn^{2+}, followed by a silver chloride scavenge. Platinum(II) was extracted into ethyl acetate. After evaporating the organic phase, platinum was reduced to the metallic state with magnesium powder in $2N$ HCl.

Gold: Gold was extracted from $6N$ HCl solution into ethyl acetate. The organic layer was transferred to a beaker containing a hydrazine hydrochloride solution, evaporated, and the metallic gold precipitate was filtered.

Mercury: Mercury was precipitated with hydrogen sulfide from $0.3N$ HCl solution, dissolved with a sodium-sulfide—sodium-hydroxide solution, and reprecipitated with ammonium chloride. After dissolving the precipitate in concentrated HCl and KI solution, mercury was precipitated with hydrogen sulfide.

Thallium: Thallium was extracted into ethyl acetate from a $6N$ HCl solution. After separation from gold (see the preceding), thallium was precipitated with sodium iodide.

Lead: Lead sulfide was precipitated from $0.3N$ HCl solution. After washing with $6N$ HCl, the lead sulfide was dissolved in concentrated HCl. Finally, lead was precipitated with sodium chromate from an ammonium acetate buffer solution.

Bismuth: A bismuth sulfide precipitation was performed from a $0.3N$ HCl solution, then dissolved in $6N$ HCl. Then a silver chloride scavenge was applied. Finally, precipitation of BiOCl was obtained by digesting a dilute hydrochloric acid solution.

Polonium: (For gamma-ray counting.) Gold and thallium were extracted into ethyl acetate from $3N$ HCl solution. Polonium was extracted from a potassium-iodide—hydrochloric-acid mixture with ethyl acetate. After back extraction with $3N$ HCl, polonium self-deposited onto a silver foil from a $0.5N$ HCl solution containing hydrazine hydrochloride. (For alpha counting.) The chemical yield of polonium in volatilization experiments to produce alpha sources was determined by the direct comparison of the ^{204}Po gamma-ray activity after the end of the alpha particle measurements with that obtained in the chemistry already described, where ^{210}Po was used as a tracer. With this method, however, the statistical error was large due to poor counting statistics. Five test runs were made with the volatilization apparatus using a known amount of ^{210}Po evaporated on an aluminum foil. The chemical yield was fairly constant, being $(83\pm4)\%$. This chemical yield was independent of whether the polonium source was placed with the activity side up or down, which means the evaporation yield is roughly independent of source depth. The reproducible chemical yield from the test runs was applied to the experimental runs, and gave answers in each case which were consistent with the ^{204}Po measurements.

*On leave from Tokyo Metropolitan University, Tokyo, Japan. Present address: Department of Chemistry, Faculty of Science, Niigata University, Niigata, Japan.

†Present address: Gesellschaft für Schwerionenforschung, Postfach 11 05 41, 6100 Darmstadt-11, Federal Republic of Germany.

[1]W. Loveland, R. J. Otto, D. J. Morrissey, and G. T. Seaborg, Phys. Rev. Lett. **39**, 320 (1977).

[2]W. Loveland, R. J. Otto, D. J. Morrissey, and G. T. Seaborg, Phys. Lett. **69B**, 284 (1977).

[3]C. R. Rudy and N. T. Porile, Phys. Lett. **59B**, 240 (1975).

[4]J. B. Cumming, R. W. Stoenner, and P. E. Haustein, Phys. Rev. C **14**, 1554 (1976).

[5]D. J. Morrissey, W. Loveland, M. de Saint Simon, and G. T. Seaborg, Phys. Rev. C **21**, 1783 (1980).

[6]S. B. Kaufman, E. P. Steinberg, B. D. Wilkins, and D. J. Henderson, Phys. Rev. C **22**, 1897 (1980).

[7]C. K. Gelbke, Nucl. Phys. **A387**, 79c (1982), and references therein.

[8]T. C. Awes, S. Saini, G. Poggi, C. K. Gelbke, D. Cha, R. Legrain and G. D. Westfall, Phys. Rev. C **25**, 2361 (1982).

[9]R. Glasow, G. Gaul, B. Ludewigt, R. Santo, H. Ho, W. Kuhn, U. Lynen, and W. F. J. Muller, Phys. Lett. **120B**, 71 (1983).

[10]M. Blann, Phys. Rev. C **23**, 205 (1981).

[11]T. J. M. Symons, P. Doll, M. Bini, D. L. Hendrie, J. Mahoney, G. Mantzouranis, D. K. Scott, K. van Bibber, Y. P. Viyogi, H. H. Wieman, and C. K. Gelbke, Phys. Lett. **94B**, 131 (1980).

[12]Ch. Egelhaaf, M. Bürgel, H. Fuchs, A. Gamp, H. Homeyer, D. Kovar, and W. Rauch, Nucl. Phys. **A405**, 397 (1983).

[13]F. Hubert, A. Fleury, R. Bimbot, and D. Gardes, Ann. Phys. (Paris) **5**, 1 (1980).

[14]A. I. Aliev, V. I. Drynkin, D. I. Leipunskaya, and V. A. Kasatkin, *Handbook of Nuclear Data for Neutron Activation Analysis* (Keter, Jerusalem, 1970).

[15]J. Kleinberg, Los Alamos Scientific Laboratory Report No. LA-1721, 1967.

[16]D. J. Morrissey, D. Lee, R. J. Otto, and G. T. Seaborg, Nucl. Instrum. Methods **158**, 499 (1979).

[17]I. Binder, R. Kraus, R. Klein, D. Lee, and M. M. Fowler, Lawerence Berkeley Laboratory Report LBL-6515, UC-34c, 1977.

[18]*Table of Isotopes,* 7th ed., edited by C. M. Lederer and V. S. Shirley (Wiley, New York, 1978).

[19]U. Reus and W. Westmeier, At. Data Nucl. Data Tables **29**, 1 (1983).

[20]M. Blann, Phys. Rev. **123**, 1356 (1961).

[21]A. C. Wahl, in *Proceedings of the International Atomic Energy Agency Symposium on the Physics and Chemistry of Fission, Salzburg, Austria, 1965* (IAEA, Vienna, 1965), Vol. I, p. 317.

[22]J. A. McHugh and M. C. Michel, Phys. Rev. **172**, 1160 (1968).

[23]C. Cabot, C. Ngo, J. Peter, and B. Tamain, Nucl. Phys. **A244**, 134 (1975).

[24]J. G. Cuninghame, J. A. B. Goodall, J. E. Freeman, G. W. A. Newton, V. J. Robinson, J. L. Durell, G. S. Foote, I. S. Grant, and J. D. Hemingway, in Proceedings of the Fourth Symposium on the Physics and Chemistry of Fission, International Atomic Energy Agency Report IAEA-SM-241/D2, 1979, p. 551.

[25]B. Borderie, M. Berlanger, D. Gardes, F. Hanappe, L. Nowicki, J. Peter, B. Tamain, S. Agarwal, J. Girard, C. Gregoire, J. Matuszek, and C. Ngo, Z. Phys. A **299**, 263 (1981).

[26]W. W. Wilcke, J. R. Birkelund, H. J. Wollersheim, A. D. Hoover, J. R. Huizenga, W. U. Schröder, and L. E. Tubbs, At. Data Nucl. Data Tables **25**, 389 (1980).

[27]G. E. Gordon, A. E. Larsh, T. Sikkeland, and G. T. Seaborg, Phys. Rev. **120**, 1341 (1960).

[28]H. C. Britt and A. R. Quinton, Phys. Rev. **120**, 1768 (1960).

[29]A. Khodai-Joopari, Lawrence Berkely Laboratory Report UCRL-16486, 1969.

[30]O. A. Zhukova, A. B. Ignatyuk, M. G. Itkis, A. I. Mul'gin, V. N. Okolovich, G. N. Smirenkin, and A. S. Tishin, Yad. Fiz. **26**, 473 (1977) [Sov. J. Nucl. Phys. **26**, 251 (1977)].

[31]F. Plasil, Oak Ridge National Laboratory Report TM-6054, 1977.

[32]H. S. Hans, M. L. Sehgel, and P. S. Gill, Nucl. Phys. **20**, 183 (1960).

[33]V. M. Abazov, M. Milanov, D. Kolev, N. Nenoff, and B. Todorov, Z. Phys. A **296**, 65 (1980).

[34]I. S. Grant and M. Rathle, J. Phys. G **5**, 1741 (1979).

[35]R. J. Prestwood and B. P. Bayhurst, Phys. Rev. **121**, 1438 (1961).

[36]R. Vandenbosch and J. R. Huizenga, Phys. Rev. **120**, 1313 (1960).

[37]Y. Nagame, H. Nakahara, and Y. Murakami, Int. J. Appl. Radiat. Isot. **30**, 669 (1979).

[38]H. Groening, K. J. Moody, and G. T. Seaborg, Nucl. Instrum. Methods **214**, 317 (1983).

[39]J. G. Cuninghame, J. A. B. Goodall, J. E. Freeman, G. W. A. Newton, V. J. Robinson, J. L. Durell, G. S. Foote, I. S. Grant, and M. Rathle, J. Phys. G **6**, 127 (1980).

[40]V. V. Volkov, in *Classical and Quantum Mechanical Aspects of Heavy Ion Collisions* (Springer, Berlin, 1975), p. 253.

[41]J. C. Jacmart, P. Colombani, H. Doubre, N. Frascaria, N. Poffe, M. Riou, J. C. Roynette, C. Stephan, and A. Weidinger, Nucl. Phys. **A242**, 175 (1975).

[42]R. Bimbot, D. Gardes, and M. F. Rivet, Nucl. Phys. **A189**, 193 (1972).